The Journal of Experimental Biology 209, 689-701
Published by The Company of Biologists 2006
doi:10.1242/jeb.02062

The relationship between 3-D kinematics and gliding performance in the southern flying squirrel, *Glaucomys volans*

Kristin L. Bishop
Department of Ecology and Evolutionary Biology, Brown University, Providence, RI 02912, USA
e-mail: Kristin_Bishop@brown.edu

Accepted 22 December 2005

Summary

Gliding is the simplest form of flight, yet relatively little is known about its mechanics in animals. The goal of this study was to describe the body position and performance of a gliding mammal and to identify correlates between kinematics and aerodynamic performance. To do this, I used a pair of high-speed digital cameras to record a portion of the middle of glides by southern flying squirrels, *Glaucomys volans*. The squirrels launched from a height of 4 m and landed on a vertical pole. Reflective markers were applied to anatomical landmarks and the 3-D coordinates of these points were computed to describe the kinematics of the glides. From these data I estimated the lift and drag generated during the glide, and correlated these variables with gliding performance as measured by glide angle, glide speed and stability. In the majority of the glide sequences the squirrels accelerated in the downward direction and accelerated horizontally forward as they moved through the calibrated volume in the middle of the glide trajectory, rather than exhibiting a steady glide in which the body weight is balanced by the resultant aerodynamic force. Compared to human engineered airfoils, the angles of attack used by the squirrels were unexpectedly high, ranging from 35.4° to 53.5°, far above the angle of attack at which an aircraft wing would typically stall. As expected based on aerodynamic theory, there was a negative correlation between angle of attack and lift coefficient, indicating that the wings are stalled, and a positive correlation between angle of attack and drag coefficient. Also as expected, there was a negative correlation between lift-to-drag ratio and angle of attack, as increasing angle of attack produced both less lift and more drag. Within glides, there was a strong correlation between nose-down pitching rotations and limb movements that tended to increase the angle of attack of the wing membrane, suggesting that the animals actively control their pitch by moving their limbs. The squirrels used much steeper glide angles than those reported for other gliding animals, ranging from 40.4° to 57.4°. It is likely that this is because they did not launch from a great enough height to reach their minimum glide angle. In some trials the glide angle increased over the captured portion of the glide, whereas in others it decreased, and the magnitude of the changes varied substantially, rendering it difficult to ascertain which portion of the glide trajectory was represented. Decreases in glide angle were strongly correlated with increases in lift coefficient, but were uncorrelated with drag coefficient.

Key words: southern flying squirrel, *Glaucomys volans*, gliding, 3-D kinematics, aerodynamic force, angle of attack, glide angle, stability.

Introduction

Gliding flight is of special interest to those who study animal locomotion for many reasons, not the least of which is its potential role as a precursor to powered flight. For example, it has been widely accepted that bats evolved from an arboreal gliding ancestor (Norberg, 1985; Norberg, 1990); however, some have suggested that an evolutionary transition from gliding to flapping flight is not mechanically possible (Caple et al., 1983). One compelling argument against a gliding-to-flapping transition is that the flapping of wings typical of gliding mammals causes fluctuations in the position of the center of pressure of the wing, introducing rotational moments that cause instability in flight. Before we can meaningfully address whether the gliding-to-flapping transition is a plausible evolutionary scenario in bats, we need to better understand the aerodynamics of extant gliding mammals. For example, an understanding of the effect of limb movements on the generation of forces and rotational moments would shed light on whether flapping is likely to introduce control problems during flight.

Gliding has evolved independently in at least six lineages of living mammals: three placental groups (Dermoptera, Sciuridae and Anomaluridae) and three marsupial families (Acrobatidae, Petauridae and Pseudocheiridae). All of these

groups share similar morphology and arboreal habits. Specifically, all living mammalian gliders have low aspect ratio wings that are nearly rectangular in shape (Stafford, 1999) and nearly all have wing membranes that extend from the wrist to the ankle (with the exception of the Pseudocheiridae, whose wing membrane attaches at the elbow and ankle). This convergence suggests that a common set of selective pressures may exist for mammalian gliding. If so, and if bat ancestors were gliding mammals, then it is reasonable to use common features of extant gliding mammals as a model for a hypothetical gliding protobat. To do this, it is essential to first describe the range of gliding behavior exhibited by living mammalian gliders and to understand how morphology and kinematics determine glide performance.

To date, the vast majority of studies of gliding in mammals have been conducted in the field without the use of video documentation (Ando and Shiraishi, 1993; Jackson, 2000; Nachtigall, 1979a; Scheibe and Robins, 1998; Scholey, 1986; Stafford et al., 2002; Vernes, 2001). Performance parameters such as airspeed and glide angle have been estimated based on the launching and landing points of the glide, and are averaged over the entire glide. Although these techniques supply useful information about the behavior of gliding animals in the wild, they do not provide the detail required to understand the aerodynamics of gliding flight and the connection between behavior and performance (for examples of detailed kinematic studies in other groups, however, see McGuire and Dudley, 2005 and Socha et al., 2005).

Gliding performance

The goal of this study was to describe the body position and performance of a gliding mammal in order to identify correlates between kinematics and aerodynamic performance. An animal may glide for any number of reasons, so the relevant measure of performance depends on what the animal is doing. For example, if the animal glides primarily to move to distant food resources, then the horizontal distance traveled from a given height is an important consideration. However, if the animal is evading a predator, then airspeed might be a more relevant measure of performance. In addition, ability to stably control the glide and maintain a desired direction are essential. Accordingly, the three measures of gliding performance considered here are the horizontal distance from a given height, velocity and stability. I use glide angle, the angle between the velocity vector and the horizontal, as a convenient measure of the horizontal distance that can be traveled from a given height. In this study I have measured instantaneous glide angle (as in Socha et al., 2005) rather than overall glide angle for the full trajectory. Performance in terms of velocity is considered here to be the magnitude of the velocity in the direction of the glide path. I use rotations about the lateral–medial axis (pitch) as a measure of stability.

The ability of an animal to control its glide trajectory and speed depends on its manipulation of aerodynamic forces. In a steady, non-accelerating glide, the gravitational force operating on the animal is balanced by a vertically oriented net aerodynamic force, which is composed of a drag component, oriented parallel and opposite in direction to the glide path, and a lift component, oriented perpendicularly to the glide path (Fig. 1). Of the determinants of lift and drag generation, the three over which a gliding animal has the most direct control are the orientation of the wing with respect to the oncoming air, the shape of the wing and how much of the wing is exposed to the airflow, i.e. the angle of attack, camber and area of the wing, respectively.

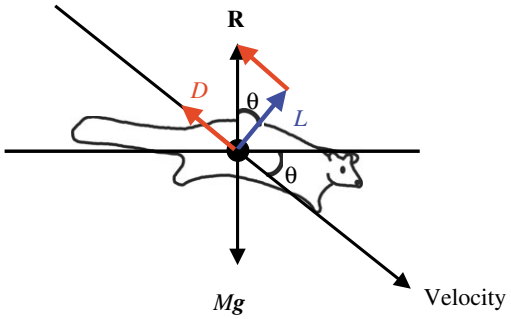

$$\theta = \arctan\frac{D}{L};\ \frac{1}{\theta} = \arctan\frac{L}{D}$$

Fig. 1. Relationship between lift-to-drag ratio and glide angle. *M*, mass of the animal; ***g***, acceleration due to gravity; **R**, resultant aerodynamic force vector; *L*, lift; *D*, drag; θ, glide angle.

Angle of attack is a measure of the orientation of a wing with respect to the direction of the air moving past it. This angle is typically defined as the angle between a line connecting the leading and trailing edge of the wing (the chord line) and the velocity vector of the oncoming fluid. In a gliding animal, the angle of attack is partially a function of the glide angle because glide angle determines the orientation of the oncoming airflow with respect to the animal, but it is also determined by the angle of the body with respect to the glide path. In addition, the wing can be held at an angle with respect to the body, changing the angle of attack of the wing. Therefore, a gliding animal can adjust its angle of attack behaviorally by moving its limbs in a way that alters the angle of the wing with respect to the oncoming airflow.

Camber is a measure of the leading edge to trailing edge curvature of a wing and is defined as the maximum distance between the chord line and an arc that is at every point equidistant from both the top and bottom surface of the wing. A gliding mammal with its wing membrane stretched between its fore- and hindlimbs can adjust the camber of its wings in one or both of two ways. The forelimb and hindlimb can be brought closer together, decreasing tension in the membrane and allowing greater billowing. In addition, gliding mammals have intrinsic musculature in the skin of the wing membrane (Johnson-Murray, 1977; Johnson-Murray, 1987) that could theoretically be relaxed or tensed to allow more or less slack in the wing.

All else being equal, larger wings generate both more lift and more drag than smaller wings, so the area of the wings

relative to the animal's body weight is an important factor in flight. Weight per unit of wing area (*Mg*/*S*) is called wing loading. During a glide, squirrels can alter their wing loading by moving their limbs in ways that change their wing area, such as flexing and extending the elbows and knees. Aerodynamic theory predicts that wing loading will be positively correlated with minimum glide speed (Norberg, 1990; Vogel, 1994) and prior studies have explored the performance consequences of wing loading in gliding snakes (Socha and LaBarbera, 2005) and lizards (McGuire and Dudley, 2005).

Linking kinematics to performance

To link kinematic behavior to gliding performance, it is important to understand how performance parameters are affected by the balance of aerodynamic forces. In this study I employ 3-D kinematic analysis to document the gliding behavior of the southern flying squirrel, *Glaucomys volans*. By so doing, I describe how flying squirrels behaviorally adjust the angle of attack and camber of their wing membranes. I use the kinematic data to estimate the lift and drag produced while gliding. These forces can then be related to changes in wing orientation and shape, as well as differences in performance as measured by glide angle, speed, and stability. This study represents the first detailed 3-D kinematic analysis of gliding in a mammal and is the first to successfully identify correlates between postural changes and gliding performance on a fine scale.

Materials and methods

Study animals and glide arenas

A colony of seven adult southern flying squirrels (*Glaucomys volans* L.) was housed at the Brown University Animal Care Facility (IACUC #62-03). These individuals were part of a long-standing research colony and had been in captivity for several years prior to these experiments. I trained the animals to glide from a launching pole resembling a thick, horizontal tree branch to a landing pole resembling a large tree trunk. Two female squirrels were reliable gliders and all of the data presented are for these two individuals (see Table 1 for morphological measurements). We reproduced this experimental arrangement in two settings: an unused stairway (Brown University, hereafter Arena 1) and a large laboratory space (Concord Field Station, Harvard University, hereafter Arena 2). The launching pole was a 5 cm diameter PVC pipe covered in window screening to provide traction. The landing pole was a 10 cm diameter PVC pipe approximately 2 m tall wrapped in carpet padding to soften the landing and provide a secure foothold. A nest box was mounted on the landing pole as an incentive for the squirrels to glide. Food was not restricted prior to the experiments. The squirrels were weighed immediately before the trials to ensure an accurate measurement of their mass during data collection. In all trials I encouraged the squirrels to launch from the launching pole and never dropped or tossed them to induce gliding. We ceased the trials when an animal refused to launch for a period of approximately 5 min. The number of recorded trials ranged from 1 to 15 per animal per day. In Arena 1 the vertical distance from the launching pole to the bottom of the landing pole was 4 m and the horizontal distance from the launching to landing pole was approximately 4.75 m, allowing a range of mean glide angles from about 20° to about 40°. Animals sometimes employed angles greater than 40° and landed on the floor, short of the landing pole. To ensure that glide distance was not constrained by the limited horizontal space in the stairway, the larger space in Arena 2 was used to allow glides of similar height, but a much longer horizontal distance than in Arena 1. The landing pole was placed farther away from the launching pole than we expected them to glide so that they landed on the floor and the length of the glide was not constrained in any way.

Table 1. *Morphological measurements and number of trials*

	IndA	IndB	Total
Mass (g)	78.1	84.0	
Wing area (m^2)	0.0204	0.0203	
Aspect ratio	1.08	1.15	
Wing loading ($N\ m^{-2}$)	41.88	47.77	
Number of glides	14	19	33
Arena 1	9	6	15
(Camber)	(5)	(0)	(5)
Arena 2	5	13	18
(Camber)	(5)	(13)	(18)

Ind, individual.

Data collection and analysis

Spherical reflective markers, approximately 6 mm in diameter, were attached to the squirrels using medical adhesive to the skin overlying the sternum, center of the pelvis, wrist, ankle and middle of the free edge of the patagium (Fig. 2). Fur was trimmed as needed to apply markers directly to the squirrels' skin and to ensure that the markers were clearly visible in the video. I designated the line connecting the wrist and ankle markers as the 'chord line', the straight-line distance between the wrist and ankle marker the 'chord length', and the line connecting the sternum and pelvis markers the 'body axis' (Fig. 2). I recorded video sequences in the middle of the glide path using two high-speed digital cameras (Redlake, PCI-1000, San Diego, CA, USA) at a framing rate of 250 Hz and an image size of 480×420 pixels. The markers were placed ventrally such that they were visible in both cameras, which were positioned below the glide path (Fig. 3). The volume of space visible in both cameras was calibrated in three dimensions using a 0.57 m×0.49 m×0.41 m premeasured calibration frame (Peak Performance, Inc., Englewood, CO, USA). I captured digital video sequences ranging in duration from 0.07 s to 0.38 s (mean 0.21 s) from the middle of 36 glides by two individuals on 4 days (2 days in each arena). Three trials were removed from all analyses as outliers because their mean

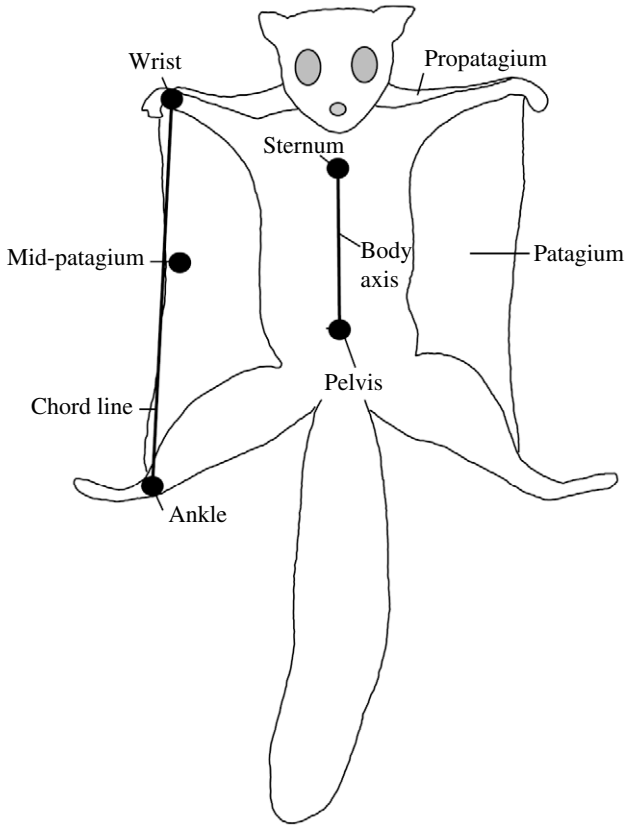

Fig. 2. Diagram of markers applied to the squirrels. The chord line is the line connecting the wrist and ankle markers; the body axis is a line connecting the sternum and pelvis markers.

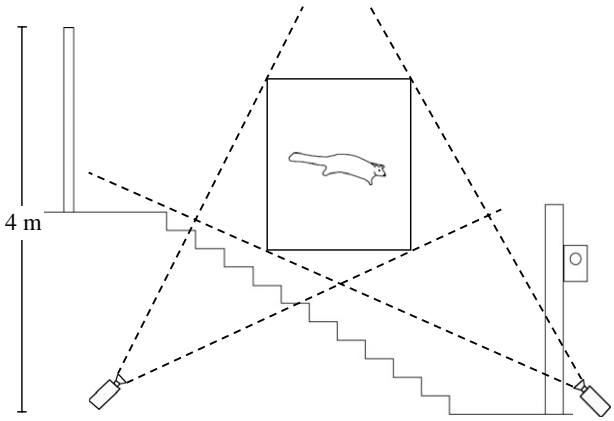

Fig. 3. Schematic of experimental setup at Brown University (Arena 1). As the squirrels glided through the calibrated volume (box), they were filmed from below by two digital cameras set at approximately 70° to one another. The setup at Concord Field Station (Arena 2) was similar, but the landing pole was positioned further away or was absent to allow the possibility of a longer horizontal glide distance.

lift-to-drag ratios were more than two standard deviations (s.d.) above the mean for all of the recorded trials. I computed camber for 23 trials in which the marker on the free edge of the patagium was visible in both cameras (Table 1). The reflective markers were digitized using kinematic analysis software (Motus version 6.1, Peak Performance, Inc.). Motus uses direct linear transformation (DLT) to compute the 3-D coordinates of each point through the glide sequence. The maximum spatial error in any dimension was 0.3%.

The squirrels' center of mass is presumed to be in the midline of the body. I used a frozen specimen to estimate the antero-posterior center of mass and found that it was very close to the center point between where the sternum and pelvis markers were placed. Because these points are coupled (assuming minimal spinal flexion) and are nearly equal distances from the center of mass, I computed the whole body velocities and accelerations as the mean between the values for the sternum and pelvis. Nevertheless, any pitching motions that the animal underwent during filming could have introduced some error in the velocity and acceleration estimates.

To compute whole body velocities and accelerations, I fit second-degree polynomials to the raw coordinate data for the sternum and pelvis markers to smooth digitizing error. Because such short periods of time were captured, these sequences were well characterized as having constant acceleration. The residual error for the polynomial fit was in the vast majority of cases well below the DLT error (maximum of 0.3%), with a maximum error of 1.2%. I computed the whole body velocity and acceleration as the first and second derivatives, respectively, of the second-degree polynomial. The estimated digitizing error was small compared to the movements of the animals, so the raw coordinate data were used for all other analyses.

The spatial resolution of the cameras when the animal was in the center of the calibrated volume was approximately 2 mm pixel^{-1}. I used a bootstrapping method to estimate the effect of small digitizing errors on the velocity and acceleration estimates. I selected four trials representing both individuals in both arenas, and for each coordinate of each time step I randomly added or subtracted a number up to 2 mm and computed the velocity and acceleration using a second degree polynomial fit. I repeated this 1000 times to generate a distribution of velocities and accelerations and computed the mean and s.d. for those distributions. The means of the 1000 trials with introduced errors matched the velocity and acceleration computed for the trial with no introduced error. The s.d. for the velocity distributions was 0.0009–0.0025 m s^{-1} and for the acceleration estimates, 0.0213–0.1056 m s^{-2}.

To assess the accuracy of the accelerations computed from the kinematic data, I dropped the same markers that were applied to the squirrels through the calibrated volume. I analyzed these sequences using the same procedures as for the squirrels and compared the computed y (vertical) component of the acceleration to gravitational acceleration. The mean vertical acceleration for these trials was 9.6±0.6 m s^{-2} (mean ± s.d.) and was not significantly different from 9.8 m s^{-2} (t-test, P=0.4396, d.f.=4).

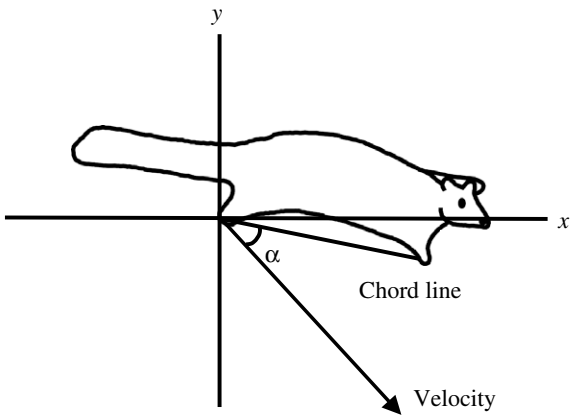

Fig. 4. Angle of attack (α) is defined as the angle between the chord line and the velocity vector of the oncoming air flow. Angle of attack was computed by subtracting the angle between the chord line and the horizontal from the angle between *x*–*y* velocity of the center of mass and the horizontal (equal to the glide angle).

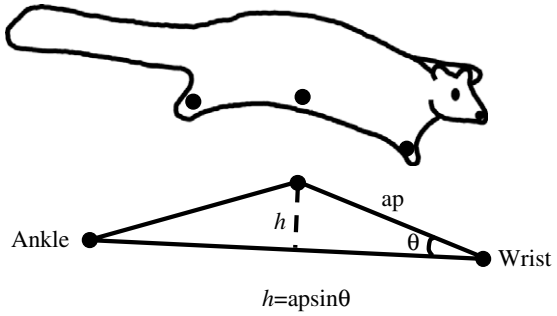

Fig. 5. Computation of camber. *h*, camber height; ap, anterior patagium length; θ, leading edge angle.

Postural adjustments to wing orientation and shape

The angle of attack was computed for each frame by subtracting the angle between the chord line and the horizontal from the angle between the velocity vector of the center of mass and the horizontal (Fig. 4). Because angle of attack depends only on inclination relative to the plane parallel to flow, angles of attack were computed in a parasagittal (*x*–*y*) plane.

To determine how the squirrels actively change their limb position in a way that affects angle of attack, I computationally rotated the coordinate system in each time step so that the *x*-axis was parallel to the body axis, and computed the difference in height between the wrist and the ankle. This removed the effect of overall body movements and allowed examination of changes in limb position with respect to the body. I conducted cross-correlation analyses to examine whether active changes in limb position are associated with changes in pitch angle, defined as the angle between the body axis and the horizontal. Cross-correlation is a statistical technique that estimates the correlation between two variables in a time series, taking into account that the effect of one variable on the other may not be instantaneous (Chatfield, 1992). Correlations are computed at a given number of positive and negative time lags, and the lag with the highest correlation coefficient is taken to be the true time lag for the relationship. This technique does not assume a causal relationship between the variables.

I estimated camber height by computing the perpendicular distance from the patagium marker to a line connecting the wrist and ankle (chord line, Fig. 5). This distance was normalized by chord length, yielding a quantity I define as relative camber. Using relative camber is useful when comparing wings of different sizes, but has the disadvantage that measurement error is compounded because two linear measurements are used. When comparing the two individuals I used relative camber to correct for differences in body size, but for camber measurements within a single glide sequence I used absolute camber height. If camber is controlled primarily by limb movements, camber should increase as the distance between the forelimb and hindlimb (chord length) decreases. I conducted a cross-correlation analysis to determine whether changes in chord length were correlated with changes in camber height. I also used a cross-correlation analysis to determine whether differences in camber are associated with changes in pitch angle.

For each time step I estimated the area of a single wing by taking the mean of the 3-D distance between the sternum and wrist and the 3-D distance between the pelvis and the ankle and multiplying it by the chord length computed for that time step, and doubled this quantity to estimate the total wing area. I computed the wing loading by dividing the weight of the squirrel measured just before the trial (mass × acceleration due to gravity) by the estimated wing area.

Estimation of aerodynamic forces

I used the *x* (forward) and *y* (vertical) components of the whole body acceleration as estimated by the mean of the accelerations measured at the sternum and pelvis to compute aerodynamic forces. In a steady, non-accelerating glide, the resultant aerodynamic force balances body weight to produce zero net vertical acceleration and is equal to the animal's body mass × acceleration due to gravity (9.8 m s^{-2}). Because the recorded glides were not steady, the *y* component of the resultant aerodynamic force was estimated by subtracting the computed vertical acceleration from gravitational acceleration, then multiplying by the animal's mass *M*:

$$a_{y,total} = \boldsymbol{g} - a_y;\ R_y = Ma_{y,total}\ , \qquad (1)$$

where *a* is acceleration, $\boldsymbol{g}$ is acceleration due to gravity, *R* is the resultant aerodynamic force, and *M* is the animal's mass. This yields the total vertical force opposing gravity, taking into account that the entire body weight may not have been supported at that time. In addition, most of the trials had a substantial acceleration in the forward direction. To compute the *x* component of the resultant aerodynamic force, I simply multiplied the *x* component of the acceleration by the squirrel's body mass. Because of the horizontal acceleration, the resultant

aerodynamic force is inclined forward as opposed to being vertically oriented as in the steady situation (Fig. 6). Because of this, in unsteady glides the glide angle does not have the relationship with lift-to-drag ratio seen in steady glides (Figs 1 and 6). By definition, drag operates in the direction opposite that of travel and lift is perpendicular to drag. I decomposed the resultant aerodynamic force into lift and drag components for each time step by computing the angle between the drag vector, which is opposite the velocity vector (Fig. 6), and the resultant aerodynamic force vector using the following equation:

$$\varphi = \arccos \frac{\mathbf{V}\cdot\mathbf{R}}{|\mathbf{V}| \times |\mathbf{R}|}, \quad (2)$$

where **V** is the opposite of the velocity vector and **R** is the resultant aerodynamic force vector. Lift and drag are computed as (see Fig. 6):

$$L = R\sin\varphi;\ D = R\cos\varphi\ . \quad (3)$$

Fig. 6 was drawn using data from a representative trial. Note that the horizontal component of lift in the forward direction is greater than the horizontal component of drag in the backward direction, hence the forward horizontal acceleration. This should be distinguished from the production of thrust, which is usually defined as being parallel and opposite to drag.

To compare airfoils of different sizes and at different speeds, lift and drag were converted to dimensionless force coefficients using the following equations (Vogel, 1994):

$$C_\mathrm{L} = \frac{2L}{\rho V^2 S};\quad C_\mathrm{D} = \frac{2D}{\rho V^2 S}$$

$$C_\mathrm{L} = \frac{2R\sin\varphi}{\rho V^2 S};\quad C_\mathrm{D} = \frac{2R\cos\varphi}{\rho V^2 S}, \quad (4)$$

where C_L and C_D are lift and drag coefficients, respectively, L=lift, D=drag, ρ=fluid density, V=velocity, S=wing area, R=resultant aerodynamic force, and φ is the reference angle between the drag vector and the resultant aerodynamic force. These coefficients must be empirically measured and serve to quantify the effects on lift and drag of factors such as angle of attack, camber, and surface properties of the wing, because these effects cannot be predicted in detail *a priori*.

Performance measures

Glide angle was computed for each time step using the following equation:

$$\theta = \arctan \frac{V_\mathrm{y}}{V_\mathrm{x}}, \quad (5)$$

where V_x and V_y are the horizontal and vertical components of the velocity, respectively, of the center of mass. This is equal to the angle that the resultant of the x and y components of velocity make with the horizontal (Fig. 1). Glide speed was estimated as the mean of the 3-D resultant velocities of the sternum and pelvis as computed by numerical differentiation of the polynomial fit of the position data. Pitch was quantified as the 3-D angle between the body axis and the horizontal.

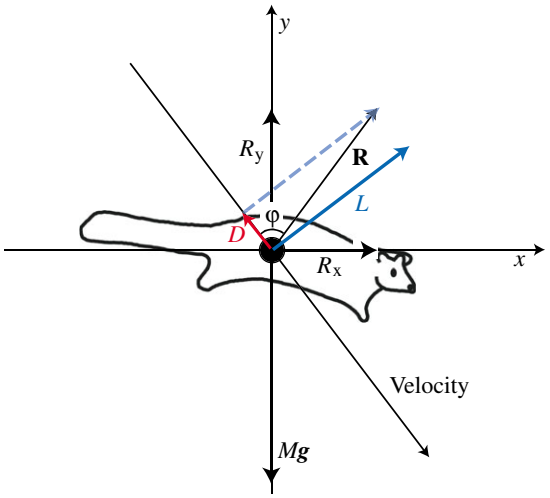

Fig. 6. Force diagram for unsteady (accelerating) glides. The resultant aerodynamic force is inclined forward because of the horizontal acceleration. A downward acceleration indicates that the vertical component of the resultant aerodynamic force has a smaller magnitude than the weight. M, mass of the animal; $\boldsymbol{g}$, acceleration due to gravity; **R**, resultant aerodynamic force vector; L, lift; D, drag; φ, reference angle between negative velocity (drag) and resultant aerodynamic force vector.

Statistics

I used the larger Arena 2, based on the prediction that the squirrels would glide farther if they had more horizontal space. Contrary to this prediction, the glides in Arena 2 were shorter for both individuals. I therefore used a two-way analysis of variance (ANOVA) with both arena and individual as factors to determine statistically significant differences in kinematic and performance variables (significance level, P=0.05). I computed Pearson correlation coefficients between the various shape parameters and performance measures (significance level, P=0.05). In cases where there are two or more variables that potentially have an effect on the performance measure of interest, I employed a stepwise multiple regression analysis to examine the contributions of each factor taking into account the effects of the other factors. All means are reported ± s.d.

Results

Postural adjustments

The cross-correlation analysis between pitch angle and limb position suggests active control of pitch stability. In 28 of the 33 analyzed trials (85%) there was a significant correlation between pitch angle and position of the wrist relative to the ankle (i.e. the angle between the chord line and the body axis, a measure of active adjustment of limb position

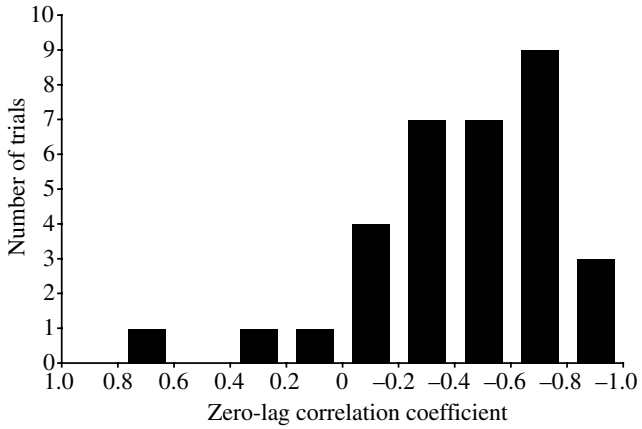

Fig. 7. Frequency distribution of the correlation coefficients at a time lag of zero for a cross-correlation analysis of limb position with pitch angle. In the majority of trials, chord angle with respect to the body axis was negatively correlated with pitch angle, such that limb movements that tend to increase angle of attack are associated with nose-down pitching moments and *vice versa*.

relative to the body) and 27 of these correlations were negative (82% of all trials), indicating that increases in pitch were associated with limb movements that tended to decrease the angle of attack (Fig. 7). In 24 of these trials the maximum correlation coefficient occurred at a lag of zero, indicating an instantaneous correlation between the two (Fig. 8). Of the remaining four trials with significant correlations, changes in limb position preceded changes in pitch angle in two (negative lag of 12 and 24 ms) and changes in pitch angle preceded changes in limb position in two (positive lag of 4 ms in both).

No consistent pattern of correlation between chord length and camber height was detected by cross-correlation, suggesting that limb movements are not a primary determinant of camber. Of the 23 trials, 17 had a significant correlation between these two variables (74%). Of these, nine were positively correlated and eight were negatively correlated. Five of the trials with significant correlation had their highest correlation coefficients at zero lag, indicating instantaneous correlation, seven had maximum correlation at negative lags (changes in chord length preceded changes in camber height) and four were most correlated at positive lags (changes in camber height preceded changes in chord length). Thus there is no consistent relationship between movements of the limbs closer together and increases in camber height.

Camber height tended to be positively correlated with pitch angle, but the correlation of pitch angle with camber height was less strong than with limb position. Pitch angle and camber height had a significant correlation in 17 of 23 trials (74%), and they were significant and positively correlated in 14 (61% of all trials). Six of the trials with a significant correlation had their maximum correlation coefficient at a time lag of zero, seven of them had a negative lag (changes in camber height preceded changes in pitch angle by 4–16 ms), and four had a positive lag (changes in pitch angle preceded changes in camber height by 8–20 ms).

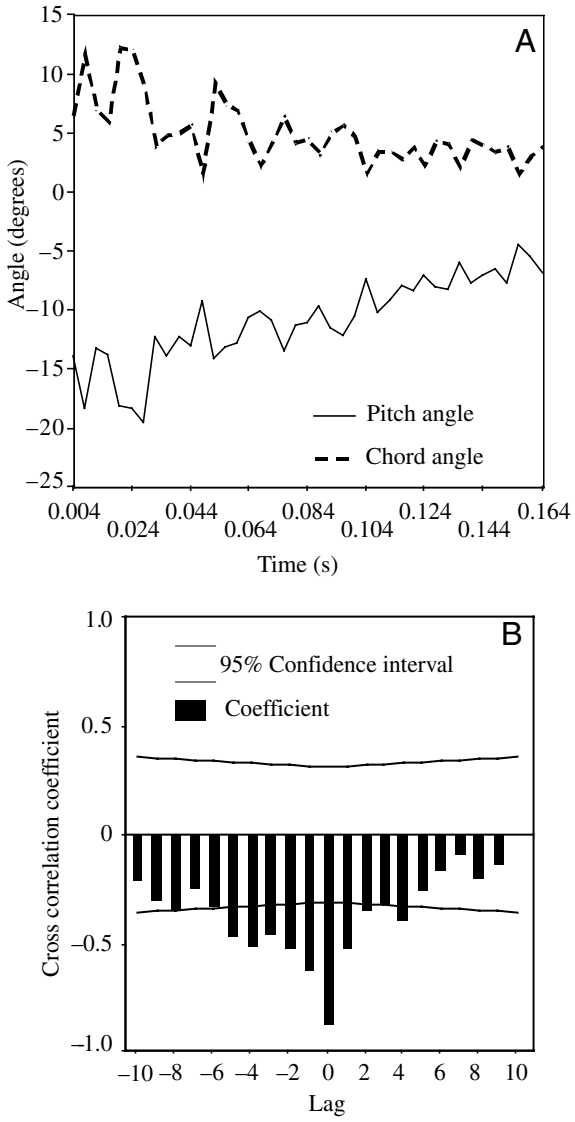

Fig. 8. (A) Pitch angle and chord angle (the angle between the chord line and the body axis, a measure of active adjustment of limb positions relative to the body) for one glide sequence. Values for pitch angle are positive when the sternum marker is higher than the pelvis marker and negative when the sternum marker is lower than the pelvis marker. The chord angle is positive when the wrist marker is higher than the ankle marker with respect to the body axis and negative when the ankle marker is higher than the wrist marker with respect to the body axis. Note that as the pitch angle increases, the chord angle decreases and *vice versa*. (B) Cross-correlogram for the same trial as in A, showing maximum negative correlation between changes in pitch angle and limb position at zero time lag. Lines represent 95% confidence interval.

Aerodynamic forces and orientation/shape

Vertical acceleration ranged from 0.7 to 5.0 m s^{-2} in the downward direction. The mean measured vertical acceleration

for all trials was 2.5±1.1 m s^{-2}, resulting in a mean vertical acceleration due to aerodynamic forces (i.e. taking into account gravity) of 7.3±1.1 m s^{-2} in the upward direction. The mean horizontal acceleration for all trials was 2.9±0.9 m s^{-2} in the forward direction. The mean lift coefficient was 2.12±0.46 and mean drag coefficient was 0.98±0.20. Squirrels used higher lift coefficients in Arena 1 than in Arena 2, and there was a significant difference in lift coefficient between the two individuals (Table 2). There was no significant difference in drag coefficient either between arenas or between individuals (Table 2).

Angle of attack

Angle of attack had strong relationships with the generation of lift and drag. The squirrels used very high angles of attack, ranging from 35.4° to 53.5° (mean=42.5±4.5°). The angles of attack used at Arena 1 were significantly lower than at Arena 2, and also differed significantly between individuals (Table 2). There was a highly significant negative correlation between angle of attack and lift coefficient and a significant positive correlation between angle of attack and drag coefficient (Table 3, Fig. 9A). Accordingly, there was a significant negative correlation between angle of attack and lift-to-drag ratio (Table 3, Fig. 9A).

Camber

For all trials pooled, camber height averaged 14±2% of chord length (relative camber=0.14). Relative camber differed significantly between the two arenas, but did not differ between individuals (Table 2). As predicted by aerodynamic theory,

Table 2. *Summary of descriptive statistics and results of two-way ANOVAs*

			Average	Individual			Arena			*P*
	IndA	IndB	for arena	*F*	d.f.	*P*	*F*	d.f.	*P*	Ind×Arena
Wing loading (N m^{-2})				102.094	1	<0.001	93.408	1	<0.001	0.002
Arena 1	45.84±1.14	51.49±2.28	48.10±3.29							
Arena 2	34.73±0.99	46.22±3.02	43.03±5.89							
Average for Ind	41.88±5.63	47.88±3.73	**45.33±5.46**							
Lift coefficient				93.581	1	<0.001	134.6	1	<0.001	0.002
Arena 1	2.25±0.12	2.66±0.17	2.42±0.25							
Arena 2	1.24±0.06	2.12±0.24	1.87±0.45							
Average for Ind	1.89±0.51	2.29±0.34	**2.12±0.46**							
Drag coefficient				0.006	1	0.941	0.028	1	0.869	0.698
Arena 1	0.97±0.17	0.99±0.19	0.98±0.17							
Arena 2	1.01±0.27	0.98±0.22	0.99±0.23							
Average for Ind	0.98±0.20	0.98±0.21	**0.98±0.20**							
Lift-to-drag ratio				12.157	1	0.002	15.109	1	0.001	0.127
Arena 1	2.39±0.42	2.77±0.42	2.54±0.45							
Arena 2	1.29±0.33	2.31±0.69	2.02±0.76							
Average for Ind	1.99±0.66	2.45±0.64	**2.26±0.68**							
Angle of attack (deg.)				21.428	1	<0.001	16.453	1	<0.001	0.849
Arena 1	43.1±4.2	37.1±1.4	40.7±4.5							
Arena 2	47.9±5.4	42.4±2.2	44.0±4.1							
Average for Ind	44.9±5.0	40.7±3.2	**42.5±4.5**							
Relative camber				3.623	1	0.071	76.741	1	<0.001	
Arena 1	0.16±0.00		0.16±0.00							
Arena 2	0.12±0.01	0.13±0.01	0.13±0.01							
Average for Ind	0.14±0.02	0.13±0.01	**0.14±0.02**							
Glide angle (deg.)				0.592	1	0.448	249.999	1	<0.001	0.004
Arena 1	43.0±0.7	41.6±1.0	42.5±1.1							
Arena 2	50.2±0.6	52.4±2.2	51.8±2.1							
Average for Ind	45.6±3.6	49.0±5.5	**47.6±5.0**							
Velocity (m s^{-1})				20.972	1	<0.001	17.948	1	<0.001	0.915
Arena 1	5.09±0.11	5.32±0.07	5.19±0.15							
Arena 2	4.87±0.20	5.11±0.15	5.04±0.19							
Average for Ind	5.01±0.18	5.18±0.16	**5.11±0.19**							

Values are means ± s.d. Values in bold are overall mean ± s.d. for all trials.
Ind, individual.

Table 3. *Pearson correlation coefficients and probabilities for position, force and performance variables*

Position and force	Angle of attack		Relative camber	
	r	*P*	*r*	*P*
Lift coefficient	–0.603	<0.001	0.447	0.032
Drag coefficient	0.472	0.006	–0.342	0.111
Lift-to-drag ratio	–0.706	<0.001	0.462	0.026

Force and performance	Lift coefficient		Drag coefficient		Lift-to-drag ratio		Wing loading	
	r	*P*	*r*	*P*	*r*	*P*	*r*	*P*
Glide angle	–0.575	<0.001	–0.041	0.821	–0.024	0.888	–0.451	0.008
Velocity	0.483	0.004	0.175	0.331	–0.283	0.094	0.476	0.005

r, Pearson correlation coefficient; *P*, probability.

there was a significant positive correlation between relative camber and lift coefficient (Table 3, Fig. 9B), but no correlation was found between relative camber and drag coefficient (Table 3, Fig. 9B). There was a significant positive correlation between relative camber and lift-to-drag ratio (Table 3, Fig. 9B).

A stepwise multiple regression analysis retained angle of attack, but removed relative camber, as factors affecting lift coefficient. Angle of attack accounted for 32.3% of the variation in lift coefficient (adjusted r^2=0.323, P=0.003, beta coefficient=–0.595). The stepwise regression model for drag coefficient also removed relative camber and retained only angle of attack as a factor. Angle of attack accounted for 31.1% of the variation in drag coefficient (adjusted r^2=0.311, P=0.003, beta coefficient=0.585). The stepwise regression model for lift-to-drag ratio retained angle of attack and removed relative camber as factors. Angle of attack accounted for 45.1% of the variation in lift-to-drag (adjusted r^2=0.451, P<0.001, beta coefficient=–0.690).

Performance – aerodynamic forces

Glide angle

Overall, the glide angles used by the squirrels were steep, with a mean for all trials of 47.6±5.0°. Glides were significantly steeper in Arena B than in Arena A (Table 2) but did not differ between individuals (Table 2). Lower glide angles were strongly associated with higher lift coefficients, but were not correlated with drag coefficient (Table 3). Squirrels used higher lift coefficients, but similar drag coefficients in Arena 1 as compared to Arena 2, and had lower

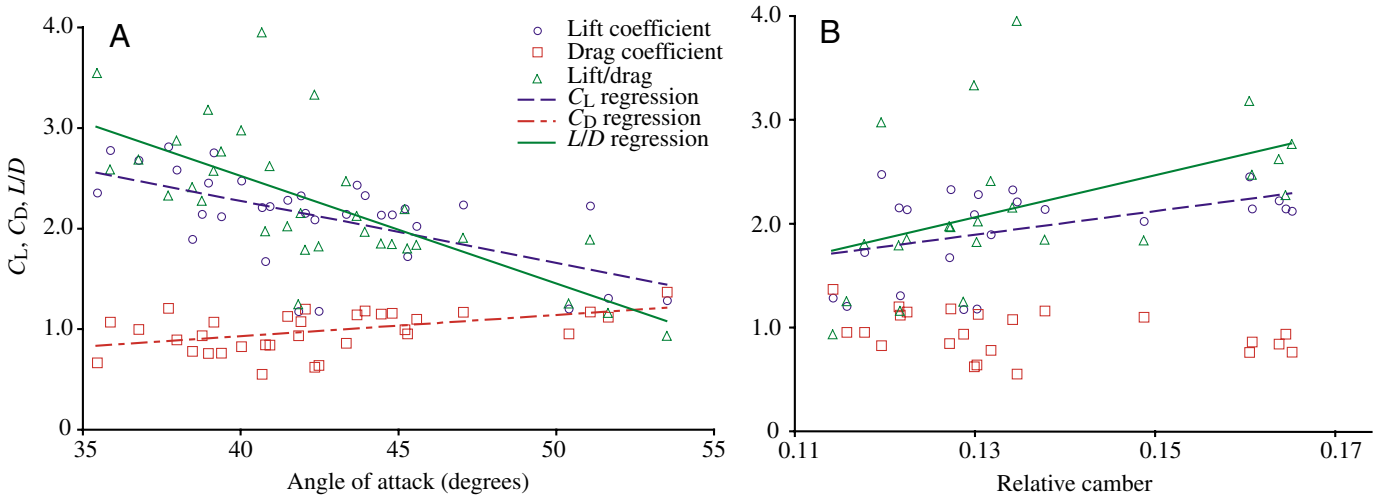

Fig. 9. (A) Coefficient of lift, coefficient of drag and lift-to-drag ratio *vs* angle of attack. Lift coefficient (y=0.0617x+4.7421) and lift-to-drag ratio (y=–0.107x+6.8044) have a significant negative correlation with angle of attack, whereas drag is positively correlated with angle of attack (y=0.0209x+0.0925). (B) Coefficient of lift, coefficient of drag and lift-to-drag ratio *vs* relative camber. Only lift coefficient (y=11.391x+0.4127) and lift-to-drag ratio (y=20.279x–0.5755) have a significant correlation with relative camber.

glide angles in Arena 1. Individual B generated more lift and similar drag coefficients as compared to Individual A, yet produced glide angles that were statistically indistinguishable.

Velocity

The mean velocity for all of the trials was 5.11±0.19 m s^{-1}. The glides in Arena 1 were faster than those in Arena 2 (Table 2). As expected, Individual 1, with a lower wing loading, glided more slowly than Individual B (Table 2). In accordance with aerodynamic theory, velocity and wing loading were significantly positively correlated (Table 3). However, contrary to theoretical expectations, velocity was positively correlated with lift coefficient. There was no correlation between velocity and drag coefficient (Table 3). Despite having a significant correlation coefficient on its own, wing loading was removed by a stepwise multiple regression model along with drag coefficient, and only lift coefficient was retained as a factor contributing to velocity. Lift coefficient accounted for 20.8% of the variation in velocity (adjusted r^2=0.208, P=0.004, beta coefficient=0.483).

Discussion

Postural adjustments

Angle of attack and stall

The most striking result of this study is the very high angles of attack used by these flying squirrels. In general, within a range of relatively low angles of attack, increasing the angle of attack increases lift as long as the fluid flow remains attached to the surface of the wing. Above a critical angle of attack, flow detaches from the surface of the wing producing aerodynamic stall, and thereafter lift decreases with increasing angle of attack. At all angles of attack between 0° and 90°, increasing angle of attack increases the drag generated by the wing as more fluid is diverted from its course. Aircraft wings typically stall at angles of attack around 15–20° (Anderson, 1985), although angles of attack much higher than the expected stall angle have also been observed in other flying and gliding animals (Dickinson et al., 1999; Socha, 2002; Socha et al., 2005; Swartz et al., 2006).

Aerodynamic theory predicts that lift coefficient should increase with increasing angle of attack up to the critical angle at which stall occurs, then should begin to decrease. Theoretically then, it is possible to determine whether a wing is stalled by looking at the empirical relationship between lift coefficient and angle of attack. In the case of flying squirrels, there is a negative correlation between lift coefficient and angle of attack (Fig. 9A), suggesting that the wings are stalled. However, the lift coefficients are much higher than would be expected for fully stalled wings.

It is possible that the squirrels' wings were not fully stalled, even at such high angles of attack. As angle of attack increases in a stalled wing, flow begins to separate from the trailing edge of the wing, but may still be attached anteriorly. There are at least two mechanisms that may help keep flow attached to the wing at higher angles of attack in flying squirrels. First is the presence of a propatagium, an extension of the wing membrane between the wrist and neck rostral to the forelimb (Chickering and Sokoloff, 1996). The propatagium can be oriented downward with respect to the rest of the wing membrane giving the wing a greater overall curvature, which can help to guide the flow more smoothly over the wing. Wind tunnel tests of physical models of pterosaur wings showed that wings with a downward deflected propatagium produced more lift than those with a reduced or no propatagium (Wilkinson et al., 2005). This effect was especially pronounced at the highest angles of attack tested, although it was not tested at angles of attack above stall. The authors attribute the improved performance to a decrease in entry angle. The entry angle is the angle between a line tangent to the leading edge and the chord line. When this angle is large, as is the case with a downward deflected leading edge flap at high angles of attack, the airflow is better able to remain attached to the wing. In addition, the ability of the flexible wing membrane to passively deform under aerodynamic loads can also help to delay stall. Comparisons between rigid and membrane wing models with a similar aspect ratio to that of flying squirrels reveal that membrane wings stall at much higher angles of attack than rigid wings (30–45° for membrane wings compared to 12–15° for rigid ones) and also attain higher maximum lift coefficients (Shyy et al., 2005). Finally, the fur covering the wing membrane can generate turbulence near the surface of the wing, helping to keep flow attached. Experiments with model wings with and without fur coverings have shown that wings with fur reach their maximum lift coefficients at higher angles of attack than similar wings without fur (Nachtigall, 1979b).

A possible explanation for the observed high lift coefficients, regardless of the degree to which the wings are stalled, lies in the squirrels having very low aspect ratio (short and broad) wings. Low aspect ratio wings have large wing tips relative to their span, which causes them to generate large tip vortices. While wing tip vorticity is generally considered detrimental to flight because it is the source of induced drag, the presence of a large vortex attached to the wing tip creates a low pressure center on the upper surface of the wing and becomes a secondary source of lift (Shyy et al., 2005; Torres and Mueller, 2001). These vortical structures have been shown to increase in strength with increasing angle of attack up to 51° (Shyy et al., 2005). Further investigation of the mechanisms for generating high lift coefficients at such high angles of attack is a compelling avenue for future research.

Angle of attack and stability

It is critical for an animal to control body rotations during a glide to maintain its glide trajectory and prevent tumbling or spinning out of control. Stability in flight is typically measured in terms of moments around the three rotational axes: pitch, roll and yaw. Pitching moments are generated on a flying body when the center of mass is either forward of or behind the center of the aerodynamic force on the wings (more commonly called the center of pressure). If the center of pressure is

forward of the center of mass, a nose-up pitching moment is generated; if the center of pressure is posterior to the center of mass the animal will tend to rotate nose-down. The position of the center of pressure depends on the distribution of lift and drag on the wing, which in turn depends on the shape and orientation of the wing membrane.

The significant correlation between pitch angle and position of the limbs relative to the body axis suggests that the squirrels actively control pitch using limb movements. The negative correlation indicates that movements that tend to increase the angle of attack of the wing are associated with nose-down rotations in pitch. This means that in the range of angles of attack used in these trials, increasing the angle of attack moves the center of pressure posteriorly, whereas decreasing the angle of attack tends to move the center of pressure anteriorly. Studies of aircraft wings show that the center of pressure moves forward as angle of attack increases up to the stalling angle, then moves backward thereafter (Dommasch et al., 1951). The finding that increases in angle of attack tend to move the center of pressure posteriorly is consistent with the wing being stalled, as expected for such high angles of attack.

Camber

Increasing camber increases the amount of lift generated by wings by enhancing the flow asymmetry between the top and bottom surfaces of the wing, as long as the airflow remains attached to the airfoil. However, because more air is diverted from a straight-line path in a more cambered wing, increasing camber is also expected to increase drag. As expected, lift coefficient was positively correlated with relative camber in these experiments, but contrary to predictions based on aerodynamic theory, there was no correlation between relative camber and drag coefficient.

If flying squirrels primarily use limb movements to control the camber of their wings, a negative correlation between the distance between the wrist and ankle and the camber height is expected. The cross-correlation analysis presented here shows that there are significant correlations between the two, but they are just as likely to be positive as negative, suggesting that flying squirrels use both limb movements and intrinsic musculature to control the shape of the wing membrane during gliding.

The variability in the correlation between pitch angle and camber height probably reflects the influence of factors other than camber on pitch angle (such as limb position). There does seem to be a small, positive relationship between camber and pitch angle in the majority of the trials such that increases in camber result in nose-up rotations in pitch. This suggests that increasing camber moves the center of pressure anteriorly on the wings.

Aerodynamic forces and performance

Glide angle

Glide angle, the angle of descent with respect to the horizontal, is related to the horizontal distance a glider can travel from a given height. In a steady glide, the glide angle is determined by the lift-to-drag ratio (Fig. 1).

$$\tan\theta = \frac{D}{L}; \quad \cot\theta = \frac{L}{D}, \tag{6}$$

where θ is the glide angle, L is lift and D is drag. To maximize the horizontal distance traveled from a given height, an animal would make its glide angle as small as possible by generating a large amount of lift relative to drag.

Gliding has traditionally been defined as non-flapping aerial locomotion at a glide angle between 0° and 45° (Norberg, 1990; Oliver, 1951; Vogel, 1994). This is typically distinguished from parachuting, which is defined as descent at an angle greater than 45°. These are not, however, mechanistically distinct behaviors. When lift and drag are equal, the glide angle is 45°. A shallower glide occurs when lift is greater than drag, resulting in a glide angle less than 45°. When drag is greater than lift the glide angle is greater than 45° and the animal descends more steeply. The range of angles of descent in non-powered flight corresponds to a continuum of lift-to-drag ratios and not distinct locomotor modes, hence I will make no distinction here between gliding and parachuting (Moffett, 2000).

The difference in mean glide angle between the trials conducted at Arena 1 and those at Arena 2 provides an opportunity to compare steeper to more shallow glides. In a steady glide, the resultant aerodynamic force is oriented vertically and glide angle is therefore directly proportional to lift-to-drag ratio (Fig. 1, Eqn 6). However, in accelerating glides, the resultant aerodynamic force can be inclined relative to the vertical as evidenced by the horizontal accelerations such that glide angle does not depend strictly on lift-to-drag ratio (Fig. 6). This accounts for the fact that in these accelerating glides, glide angle had no correlation with lift-to-drag ratio and more shallow glides were associated only with increased lift coefficients (Table 3). The shorter glides in Arena 2 were surprising given the greater horizontal space available, and may be due to a shorter period of training at Arena 2.

Field estimates of glide angle in the closely related and similarly sized northern flying squirrel (*Glaucomys sabrinus*) averaged 26.8°, corresponding to a mean lift-to-drag ratio of 1.98 (Vernes, 2001), presuming a steady glide. The mean net height loss for these glides was 10.2 m, compared to 4 m in our experiments. It is likely that the squirrels in this study did not launch from a great enough height to reach their minimum glide angle. The expected glide trajectory for mammals begins with a relatively steep glide angle until the animal has reached a sufficiently high speed to maximize its lift. When this steady speed is reached, the glide angle is expected to become constant until the animal is about to land, at which time the animal rises slightly as it rapidly increases its angle of attack in order to orient itself such that it can land on the vertical trunk of the landing tree. In the present study, the squirrels did not exhibit steady glides. According to the predicted glide trajectory described above, the fact that the squirrels in this

study were accelerating as they moved through the calibrated volume suggests that the initial acceleration phase occurs over at least the first two vertical meters (the approximate position of the calibrated space in this experiment). It is also possible that squirrels regularly adjust their glide angle and speed throughout the glide depending on their intended target, and that there is no characteristic steady phase. Despite the fact that the same volume of space was captured for each glide sequence relative to the launching and landing points, there was no consistent pattern of increase or decrease in the glide angle. Thus, it is impossible to determine with certainty which part of the glide trajectory is represented. This lends support to the idea that glides may not typically include the predicted steady phase and that glide angle may be adjusted continuously. A plot of horizontal glide distance *vs* net height loss in Vernes (2001) field study suggests that glides with shorter horizontal distances tend to have relatively greater losses in height; in other words, short glides tend to have larger glide angles. However, these estimates are not strictly comparable to the data from this study because they represent an average glide angle over the whole trajectory rather than instantaneous glide angle for a short segment during mid-glide.

Velocity

Glide speed depends on the animal's weight relative to its wing area and also on the force coefficients it generates. Theoretical calculations of minimum glide speed in the animal gliding literature usually assume that glide angles are very small and that lift is nearly equal to the weight of the animal (Norberg, 1990; Vogel, 1994). Substituting the weight of the animal for lift in the formula for lift coefficient given above and rearranging to solve for velocity, gives:

$$V_g = \sqrt{\frac{2Mg}{C_L \rho S}}, \quad (7)$$

where V_g is the glide velocity, M is the mass of the animal, and g is acceleration due to gravity. Thus, the minimum glide speed depends on the animal's wing loading, or weight per unit wing area (Mg/S); the greater the wing loading, the faster the animal's glide speed. It also follows from this equation that to minimize glide speed, an animal must maximize its lift coefficient, and conversely that lower lift coefficients lead to faster glides (Norberg, 1990).

The assumption of very small glide angles may not cause large errors in the case of soaring birds or the most specialized gliding mammals, but the majority of gliding animals use glide angles that differ substantially from zero. In non-accelerating glides the resultant aerodynamic force is equal to body weight, so as glides become steeper, equating lift to weight becomes a poorer approximation because drag makes a greater contribution to the aerodynamic force balancing the body weight. Because the resultant aerodynamic force is the sum of lift and drag vectors, both of which vary with the square of velocity, wing area and air density, we can define a resultant coefficient of force, C_F based on Eqn 4. Substituting body weight for the resultant force and solving for velocity gives:

$$V_g = \sqrt{\frac{2Mg}{C_F \rho S}}, \quad (8)$$

where C_F is the coefficient of the resultant aerodynamic force. Velocity still depends on wing loading (Mg/S), but in this case the force coefficient reflects effects of both lift and drag coefficients and maximizing C_F minimizes glide speed.

According to the analysis above, it is appropriate to consider the roles of wing loading, lift coefficient and drag coefficient as possible factors influencing glide velocity. Although there was a significant correlation between wing loading and velocity when analyzed separately, the stepwise multiple regression analysis indicates that the only significant predictive factor of velocity is lift coefficient. McGuire and Dudley (McGuire and Dudley, 2005) also found no significant correlation between velocity and wing loading in an interspecies comparison within gliding lizards (genus *Draco*), which the authors attribute to low statistical power. The present study also found relatively low correlation between velocity and wing loading, but found that the variation in velocity is explained by variation in coefficient of lift.

Conclusions

Understanding the interrelationships between structure, function and performance is critical to our ability to frame meaningful questions about the role of locomotion in the evolution and ecology of animals. The problem of how to quantify performance in animal locomotion has been a persistent one because the relevant performance parameters are context dependent. Clearly, horizontal distance traveled, speed and stability are all potentially important ecologically for gliding mammals and care must be taken to specify the relevant component of performance in the context of a particular activity. It is also crucial in models of optimization of performance to consider possible trade-offs for different kinds of performance. For example, in the case of gliding mammals, maximizing lift-to-drag ratio may have consequences for stability (K.L.B., unpublished data).

Similarly, a clear understanding of the relationship between kinematics and performance is critical to our ability to form hypotheses about the evolutionary history of locomotion. For example, we cannot begin to address the role of stability in the evolution of flapping flight without understanding the role of postural changes in rotational movements (Caple et al., 1983; Essner, 2002). The results of this study suggest that active movements of the wing membrane in gliders may be important in maintaining aerodynamic stability, so it is possible that small amplitude 'flapping' behavior in preflight bat ancestors might have enhanced stability rather than diminishing it.

Because this study looks at only a small segment of the glide and it is unknown what particular part of the glide trajectory it represents, the conclusions that can be drawn about the ecological relevance of these results are limited. Much additional information could be gained by placing results such

as these in the context of whole glide trajectories. However, a detailed view of a small segment of a glide provides valuable and novel information about the aerodynamics of gliding and raises many fascinating questions about the properties of compliant wings. This study is an important first step toward understanding the aerodynamic properties of mammalian wings and how these properties relate to gliding performance.

List of symbols

a	acceleration
ap	length of anterior segment of patagium
α	angle of attack
C_D	coefficient of drag
C_F	coefficient of resultant aerodynamic force
C_L	coefficient of lift
D	drag
φ	reference angle between drag and resultant aerodynamic force
$\boldsymbol{g}$	acceleration due to gravity
h	camber height
L	lift
M	mass
R	resultant aerodynamic force
$\mathbf{R}$	resultant aerodynamic force vector
ρ	density
S	wing area
θ	glide angle
V	velocity
$\mathbf{V}$	velocity vector

I am grateful to W. Brim-deForest and K. Stellmach for extensive assistance in animal training and data collection. Additional assistance with data collection was provided by J. Hamilton, K. Middleton, J. Iriarte-Diaz, and A. Sullivan. Thanks also to A. Biewener and the staff at Concord Field Station for providing access to their facilities and to T. Hedrick for help with equipment and extensive advice on kinematic analysis. Thanks to D. Ritter for assistance with building equipment and to J. Witman, J. Iriarte-Diaz and E. Von Wettberg for help with statistics. Brown University Animal Care Facility provided support and services above and beyond the call of duty. I thank S. Swartz, K. Breuer, S. Gatesy, T. Roberts, E. Brainerd, C. Janis, K. Middleton, D. Ritter, D. Baier, J. Hamilton, J. Iriarte-Diaz, A. Clifford, F. Nelson and J. Socha for comments and discussion of this work. This manuscript was greatly improved by the comments of two anonymous reviewers.

References

Anderson, J. D. (1985). *Introduction to Flight*. New York: McGraw-Hill.

Ando, M. and Shiraishi, S. (1993). Gliding flight in the Japanese giant flying squirrel *Petaurista leucogenys*. *J. Mamm. Soc. Jpn.* **18**, 19-32.

Caple, G., Balda, R. P. and Willis, W. R. (1983). The physics of leaping animals and the evolution of preflight. *Am. Nat.* **121**, 455-476.

Chatfield, C. (1992). *The Analysis of Time Series: An Introduction*. London, New York: Chapman and Hall.

Chickering, J. G. and Sokoloff, A. J. (1996). Innervation of propatagial musculature in a flying squirrel, *Glaucomys volans* (Rodentia, Sciuridae). *Brain Behav. Evol.* **47**, 1-7.

Dickinson, M. H., Lehmann, F.-O. and Sane, S. P. (1999). Wing rotation and the basis of insect flight. *Science* **284**, 1954-1960.

Dommasch, D. D., Sherby, S. S. and Connolly, T. F. (1951). *Airplane Aerodynamics*. New York: Pitman Publishing.

Essner, R. L. (2002). Fluttering: a novel locomotor behavior in flying squirrels. *Integr. Comp. Biol.* **42**, 1227.

Jackson, S. M. (2000). Glide angle in the genus *Petaurus* and a review of gliding in mammals. *Mamm. Review* **30**, 9-30.

Johnson-Murray, J. L. (1977). Myology of the gliding membranes of some petauristine rodents (genera: *Glaucomys*, *Pteromys*, *Petinomys*, and *Petaurista*). *J. Mamm.* **58**, 374-384.

Johnson-Murray, J. L. (1987). The comparative myology of the gliding membranes of *Acrobates, Petauroides* and *Petaurus* contrasted with the cutaneous myology of *Hemibelideus* and *Pseudocheirus* (Marsupialia: Phalangeridae) and with selected gliding Rodentia (Sciuridae and Anamoluridae). *Austr. J. Zool.* **35**, 101-113.

McGuire, J. A. and Dudley, R. (2005). The cost of living large: Comparative gliding performance in flying lizards (Agamidae: Draco). *Am. Nat.* **166**, 93-106.

Moffett, M. W. (2000). What's 'up'? A critical look at the basic terms of canopy biology. *Biotropica* **32**, 569-596.

Nachtigall, W. (1979a). Gliding flight in *Petaurus breviceps papuanus*. II. Cine film analysis of gliding path, trunk position and steering of gliding. *J. Comp. Physiol. A* **133**, 89-95.

Nachtigall, W. (1979b). Gliding flight in *Petaurus breviceps papuanus*. III. Model measurements of the influence of fur cover on flow and generation of aerodynamic force components. *J. Comp. Physiol. A* **133**, 339-349.

Norberg, U. M. (1985). Evolution of vertebrate flight: An aerodynamic model for the transition from gliding to active flight. *Am. Nat.* **126**, 303-327.

Norberg, U. M. (1990). *Vertebrate Flight: Mechanics, Physiology, Morphology, Ecology and Evolution*. Berlin, Heidelberg: Springer-Verlag.

Oliver, J. A. (1951). 'Gliding' in amphibians and reptiles, with a remark on an arboreal adaptation in the lizard, *Anolis carolinensis carolinensis* Voigt. *Am. Nat.* **85**, 171-176.

Scheibe, J. S. and Robins, J. H. (1998). Morphological and performance attributes of gliding mammals. In *Ecology and Evolutionary Biology of Tree Squirrels* (ed. M. A. Steele, J. F. Merritt and D. A. Zegers), pp. 131-144. Virginia: Virginia Museum of Natural History.

Scholey, K. (1986). The climbing and gliding locomotion of the giant red flying squirrel *Petaurista petaurista* (Sciuridae). In *Bat Flight*, *BIONA Report 5* (ed. W. Nachtigall), pp. 187-204. Stuttgart: Gustav Fischer.

Shyy, W., Ifju, P. and Viieru, D. (2005). Membrane wing-based micro air vehicles. *Appl. Mech. Rev.* **58**, 283-301.

Socha, J. J. (2002). Gliding flight in the paradise tree snake. *Nature* **418**, 603-604.

Socha, J. J. and LaBarbera, M. (2005). Effects of size and behavior on aerial performance of two species of flying snakes (*Chrysopelea*). *J. Exp. Biol.* **208**, 1835-1847.

Socha, J. J., O'Dempsey, T. and LaBarbera, M. (2005). A 3-D kinematic analysis of gliding in a flying snake, *Chrysopelea paradisi*. *J. Exp. Biol.* **208**, 1817-1833.

Stafford, B. J. (1999). Taxonomy and ecological morphology of the flying lemurs (Dermoptera, Cynocephalidae). PhD dissertation, The City University of New York, USA.

Stafford, B. J., Thorington, R. W. and Kawamichi, T. (2002). Gliding behavior of Japanese giant flying squirrels (*Petaurista leucogenys*). *J. Mammal.* **83**, 553-562.

Swartz, S. M., Bishop, K. L. and Ismael Aguirre, M.-F. (2006). Dynamic complexity of wing form in bats: implications for flight performance. In *Functional and Evolutionary Ecology of Bats* (ed. A. Zubaid, G. F. McCracken and T. H. Kunz), pp. 110-130. New York: Oxford University Press.

Torres, G. E. and Mueller, T. J. (2001). Aerodynamics of low aspect ratio wings at low Reynolds numbers. In *Fixed and Flapping Wing Aerodynamics for Micro Air Vehicle Applications*, vol. 195 (ed. T. J. Mueller), pp. 115-142. Reston (VA): AIAA.

Vernes, K. (2001). Gliding performance of the northern flying squirrel (*Glaucomys sabrinus*) in mature mixed forest of eastern Canada. *J. Mammal.* **82**, 1026-1033.

Vogel, S. (1994). *Life in Moving Fluids*. Princeton: Princeton University Press.

Wilkinson, M. T., Unwin, D. M. and Ellington, C. P. (2005). High lift function of the pteroid bone and forewing of pterosaurs. *Proc. R. Soc. Lond. B* **273**, 119-126.